Free-Fixed Rotational Triboelectric Nanogenerator for Self-Powered Real-Time Wheel Monitoring

Long Jin, Steven L. Zhang, Sixing Xu, Hengyu Guo, Weiqing Yang,* and Zhong Lin Wang*

Developing an applicable triboelectric nanogenerator (TENG) for train wheel energy harvesting is a key step to meet the urgent need of wheel safety monitoring. Herein, an innovative design of free-fixed TENG (FF-TENG) is reported, without a serious negative impact on the wheel. The key of this design is the magnets fixed on the device and bogie, providing attractive force to immobilize the stator. With a rotational structure, FF-TENG can provide a high short-circuit current of 55 µA, an open-circuit voltage of 500 V, and a charge of 235 nC at a rotation speed of 400 rpm. At an external load resistance of 10 MΩ, FF-TENG delivers the maximum power of 15.68 mW. Furthermore, the superior robustness of FF-TENG in vibration environment is proved. In addition, a power management circuit designed by LTC 3588 is tested for more efficient capacitor charging, leading to better performance to power electronics. Finally, a self-powered real-time wheel temperature and wheel speed monitoring system is developed with FF-TENG as a safety alert demo for feasibility demonstration. Given the rational structure design and high performance, this work paves a practical way for TENGs in the field of intelligent transportation.

Dr. L. Jin, Dr. S. L. Zhang, S. Xu, Prof. H. Guo, Prof. Z. L. Wang
School of Materials Science and Engineering
Georgia Institute of Technology
Atlanta, GA 30332, USA
E-mail: zlwang@gatech.edu
Dr. L. Jin, Prof. W. Yang
Key Laboratory of Advanced Technologies of Materials (Ministry of Education)
School of Materials Science and Engineering
Southwest Jiaotong University
Chengdu 610031, China
E-mail: wqyang@swjtu.edu.cn
Prof. H. Guo
Department of Applied Physics
State Key Laboratory of Power Transmission Equipment and System Security and New Technology
Chongqing University
Chongqing 400044, China
Prof. Z. L. Wang
Beijing Institute of Nanoenergy and Nanosystems
Chinese Academy of Sciences
Beijing 100085, China

1. Introduction

Transportation has always been necessary for propelling the development of human civilization.[1,2] For example, railway networks save much time and bring immeasurable economic benefits.[3] As a common sense, safety is a precondition for railway operation. Consequently, as a crucial and wear-prone component, wheel attracts considerable attention due to its health and stability monitoring.[4–6] However, the sensors for detection are usually powered by traditional cables, requiring wear-proof collecting rings with complex wire management. On the other hand, although energy storage devices including batteries and supercapacitors have a rapid development these years,[7–11] they constantly need to be replaced and cause potential environment damage due to the toxic materials used in the fabrication process. As the world entering the era of internet of things (IoTs),[12–14] self-powered technology for sensors by harvesting environment energy is derived since the power needed to operate each sensor is small.[15–21]

Self-powered technology by triboelectric nanogenerators (TENGs) shows great potential for distributed power sources with advantages of cost effective, light weight, and high conversion efficiency.[18,22–27] Moreover, large amounts of mechanical energy on wheels are proved to be harvested by TENGs, according to previous works.[28–30] Even so, the development of TENGs for train wheels is still hindered because of the special structure of train. Widely applied in many fields, TENG is highlighted for its variable structure in special application environment, such as medicine,[31,32] constructions,[33,34] blue energy,[35–37] and so on. In this regard, designing a new structure of TENG for acclimatization is highly desirable and mandatory.

In this work, we proposed a free-fixed TENG (FF-TENG) with rotation mode for wheel train monitoring by fixing magnets on the stator and bogie. Thus, the stator is not fixed directly on the bogie, without a serious negative impact on the wheel. The magnetic force not only immobilizes the stator, but also increases the contact areas between the stator and rotator to improve output. With the rational structure design, FF-TENG delivers a short-circuit current of 55 µA, an open-circuit voltage

**ADVANCED
SCIENCE NEWS**
www.advancedsciencenews.com

**ADVANCED
MATERIALS
TECHNOLOGIES**
www.advmattechnol.de

of 500 V, and a charge of 235 nC at rotation speed of 400 rpm. At an external load resistance of 10 MΩ, the maximum power of 15.68 mW is obtained. In view of the train running environment, the device was tested on different vibration frequencies, and the result shows extreme robustness, demonstrating the great adaptability in severe environment. Finally, by integrating the device, power management circuit, a capacitor, and a wireless sensor, a system to monitor the wheel temperature in real time without an external power source was developed. It is also worth mentioning that the power management circuit in this system is designed by LTC 3588 with less charge time, rather than rectifiers. Given the special structure design and high output, this work paves a practical way for TENGs in the field of intelligent transportation, especially wheel monitoring.

2. Results and Discussion

FF-TENG is designed mainly for train wheel energy harvesting when a train is running, as shown in **Figure 1**a. As a convenience, the signals from FF-TENG powered sensor can be received indoor, for example, in the operation room. In details, FF-TENG is fixed on the principal axis concentrically (Figure 1b), which makes FF-TENG work synergistically with principal axis rotating. Ignoring inefficient and easy-wearing collecting rings, electric wires are able to connect FF-TENG and sensor together directly. Figure 1c shows the photograph of FF-TENG. For better understanding, each part of FF-TENG is illustrated in Figure 1d. As a positive layer, blade-shape polyurethane (PU) is adhered to an acrylic plate, creating the stator element of the design. In addition, two sets of magnets as fixators are adhered on the other side of the acrylic plate. Correspondingly, another set of magnets are fixed on bogie, creating an attractive force with the magnets on the stator. Therefore, the stator will not move due to the magnetic attractive force, which is the key idea of this design. The rotator element includes a polytetrafluoroethylene (PTFE) film as negative layer, blade-shape copper as electrodes, and acrylic cylindrical case. In general, the structure design of this work is similar to classical rotation TENG structure,[38–41] with the status of rotator and
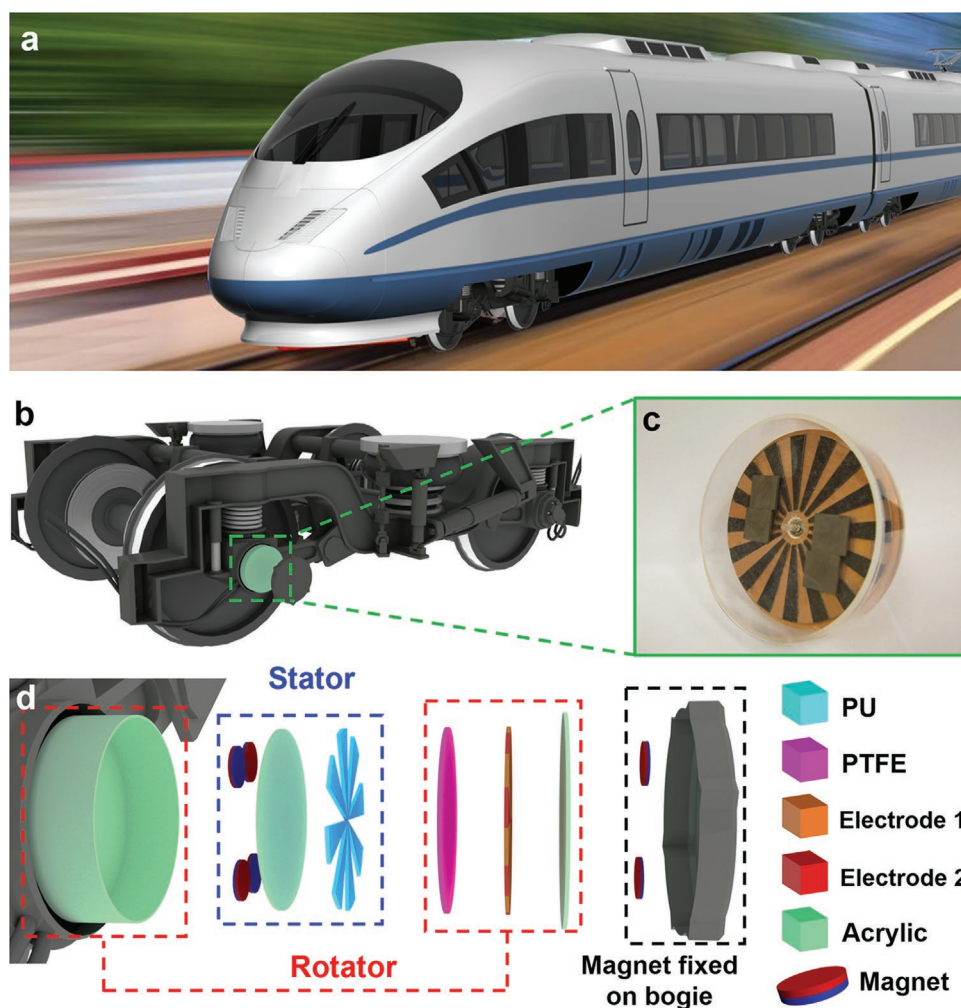

Figure 1. Structure design of FF-TENG and application for self-powered train wheel monitoring. a) Schematic illustration of FF-TENG applied on the running train. b) The detailed schematic diagram of bogie and wheel with FF-TENG. c) Photograph and the d) detailed structure design of the fabricated FF-TENG.
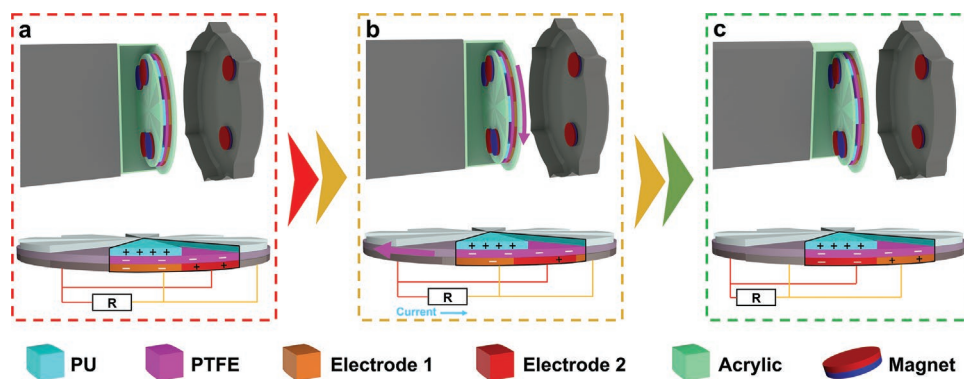
**ADVANCED
SCIENCE NEWS**

www.advancedsciencenews.com

**ADVANCED
MATERIALS
TECHNOLOGIES**

www.advmattechnol.de

Figure 2. The moving process of wheel and electricity generation process of FF-TENG. a) The initial state showing motionless wheel with an electrostatic balance between two electrodes. b) The wheel starts to move with rotator moving, leading to imbalance between two electrodes. c) After specific angle rotation, a new balance between two electrodes is achieved.

stator interchanged. Benefited by the proper structure design, the rotator and wheel move synchronously, with simple wire arrangement.

For better understanding, the working principle is illustrated in **Figure 2**. At the initial state, PU is aligned with copper electrode 1 in Figure 2a, where there is an electrostatic balance between two electrodes. Herein, magnets play a significant role with polarity, as shown in Figure S1a in the Supporting Information. Magnet 1 and magnet 2 are fixed together on the stator, while magnet 3 is fixed on the bogie (Figure S1b, Supporting Information). Meanwhile, Figure S1c in the Supporting Information demonstrates the balance state of magnets, leading to motionless rotator. Then, when the rotator is moving along with moving wheel, electrons flow from electrode 1 to electrode 2, due to the unbalanced electrostatic state (Figure 2b). In this process, stator has a trend to move because

of the friction between PTFE and PU, which is blocked by this ingenious design. As indicated in Figure S1d in the Supporting Information, when magnets have a slight relative displacement, the force between magnet 1 and magnet 3 is enhanced. At the same time, the force direction has a slight change, resulting in a horizontal component of the force. On the other hand, the force between magnet 2 and magnet 3 is enhanced, causing an enhanced horizontal component force. As a result, the stator with magnet 1 and magnet 2 has a horizontal force with opposite direction to avoid the movement. Only with this ingenious structure design, FF-TENG is workable. Finally, PU is aligned with electrode 2, inducing a new balance, as indicated in Figure 2c. Thus, short-circuit current is generated owing to electrons flowing between two electrodes.

To examine the performance of energy harvesting, a series of characterizations were conducted. **Figure 3**a shows the
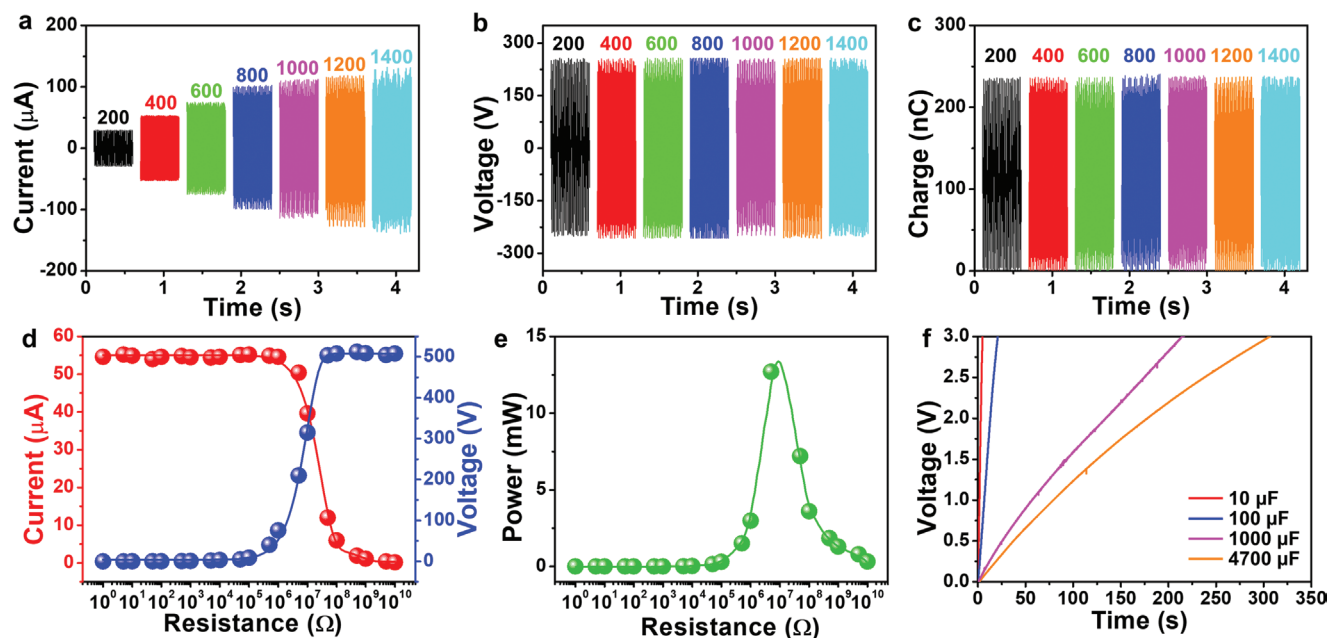

Figure 3. Output performance of FF-TENG. a) Short-circuit current, b) open-circuit voltage, and c) transferred charge of FF-TENG with various rotation speeds. d) Measured output current, voltage, and e) calculated power on different external loading resistances at the rotation speed of 400 rpm. f) The voltage of different capacitors when charged through rectifier by FF-TENG at a rotation speed of 400 rpm.

**ADVANCED
SCIENCE NEWS**
www.advancedsciencenews.com

**ADVANCED
MATERIALS
TECHNOLOGIES**
www.advmattechnol.de

short-circuit current of FF-TENG with different rotation speed from 200 to 1400 rpm. It is obvious that short-circuit current increases with increasing rotation speed. With a different trend, open-circuit voltage (peak-to-peak voltage) and transferred charge maintain about 500 V and 235 nC, respectively, when rotation speed changes, as shown in Figure 3b,c. This is the inherent performance of rotation TENG with detailed model in Figure S2 in the Supporting Information and following equations of open-circuit voltage (V) and transferred charge (Q)[38]

$$V = \frac{d \cdot \sigma}{\varepsilon_0 \cdot \varepsilon_r} \left(\frac{\alpha_0 - \alpha}{\alpha} - \frac{\alpha}{\alpha_0 - \alpha} \right) \tag{1}$$

$$Q = \frac{\alpha_0}{180} \cdot \sigma \cdot \pi \cdot \left(r_2^2 - r_1^2 \right) \tag{2}$$

where d is the thickness of PTFE layer, σ is the triboelectric charge density on PTFE layer, ε_0 is the dielectric constant of vacuum, ε_r is the relative dielectric constant of PTFE, α is the angle away from the initial state, α_0 is the central angle of single unit, and r_2 and r_1 are the outer radius and inner radius of FF-TENG, respectively. According to Equations (1) and (2), open-circuit voltage and transferred charge are stable when rotation speed changes, because the area is unchanged.

For superior application in energy harvesting, FF-TENG was tested at rotation speed of 400 rpm with external load resistances from 1 Ω to 10 GΩ. Figure 3d shows the result that current and voltage remain unchanged until load resistance increases to 1 MΩ. Between 1 and 100 MΩ, the measured current has a sharp decrease while the measured voltage has a sharp increase. Next, the current and voltage keep stable after 100 MΩ. Consequently, the maximum power of 15.68 mW (as calculated in the Supporting Information) is obtained at a resistance of 10 MΩ, as can be seen in Figure 3e. To demonstrate the charging performance, a key step of charging capacitors was taken. Figure 3f presents different capacitors charged by FF-TENG through a rectifier at rotation speed of 400 rpm.

When applying FF-TENG on train wheel, vibration environment mainly induced by loose track connection (**Figure 4**a) and rough surface (Figure 4b) has to be taken into account. Accordingly, a systematic study was performed by a vibration provider, in which different vibration frequency were tested. Figure 4c shows 3D graph of short-circuit current with different vibration frequencies from 0 Hz (nonvibration state) to 50 Hz and rotation speeds from 200 to 1400 rpm. Individually, 2D graph in Figure 4d demonstrates a few changes of short-circuit current with various vibration frequencies while rotation speed affects vastly. Figure 4e gives a clear view of increasing short-circuit current with a rotation speed growth. Moreover, the almost coincident curves further prove short-circuit current stability with different vibration frequencies. On the other hand, open-circuit voltage shows a flat surface with tiny fluctuation in Figure 4f, indicating the scarce effects on open-circuit voltage from both vibration frequency and rotation speed. Furthermore, the curves in Figure 4g,h coincide virtually, as concrete proof. Similarly, transferred charge follows the same trend with open-circuit voltage (Figure 4i–k), because transferred charge cannot be affected by rotation speed as proved by Equation (2).

Therefore, FF-TENG is demonstrated remarkably stable in vibration environment, with negligible output changes, which is the basic for wheel energy harvesting.

After comprehensive investigation of electric performance, FF-TENG needs to be utilized to power electronics for feasibility testing. Figure S3 in the Supporting Information demonstrates that 160 commercial LEDs can be lighted up sparklingly by FF-TENG at a rotation speed of 400 rpm (Movie S1, Supporting Information). For power supply continuity verification, **Figure 5**a illustrates the application scenario of FF-TENG powering a temperature sensor. When the train is braking, the friction between wheel and track raises temperature sharply (Figure 5b). Hence, a self-powered real-time temperature monitoring system was developed, including FF-TENG, a power management circuit, capacitor, sensor, signal transmitter, and a signal receiver, as shown in Figure 5b. The detailed circuit diagram is revealed in Figure S4a in the Supporting Information. It is worth mentioning that LTC 3588 (circuit diagram in Figure S4b in the Supporting Information) was used as a more efficient power management rather than utilizing just rectifiers. Figure S5 in the Supporting Information is the voltage of different capacitors charged through LTC 3588 by FF-TENG at rotation speed of 400 rpm. In details, Figure S6a in the Supporting Information presents the different voltage curves of 10 µF capacitor charged through LTC 3588 and a rectifier, indicating that rectifier can charge 10 µF capacitor faster than LTC 3588. Because the power management by LTC 3588 needs to precharge a small capacitor in the circuit. Subsequently, when 10 µF capacitor is replaced into 100 µF, the charge curve in Figure S6b in the Supporting Information shows a higher charge efficiency of LTC 3588 compared to that of the rectifiers. It is more obvious in the charge process of 1000 µF (Figure S6c, Supporting Information) and 4700 µF capacitors (Figure S6d, Supporting Information) that utilizing power management circuit by LTC 3588 is more effective.

Therefore, the self-powered wheel temperature monitoring system runs stably with the high-performance FF-TENG and high effective power management (shown in Figure 5d and Movie S2 in the Supporting Information). Figure 5e is the system interface designed by LabVIEW, including temperature data collection and alarm. Once the temperature is beyond the threshold value (50 °C in this work), it will alarm in case of emergencies. Figure 5f shows that the red curve indicates warning (beyond 50 °C) while black curve indicates safe condition (lower than 50 °C). In addition, FF-TENG with regular waveform (Figure S7, Supporting Information) was also utilized as a wheel speed sensor (Movie S3, Supporting Information). Figure S8a in the Supporting Information shows the results of fast Fourier transform (FFT) analysis from 200 to 1400 rpm. And, the calculated frequency has a terrific linear relationship with actual rotation speed, as shown in Figure S8b in the Supporting Information. Herein, a self-powered speed monitoring system by LabVIEW (Figure S8c, Supporting Information) was also developed with system algorithm flow chart in Figure S8d in the Supporting Information. As a consequence, FF-TENG not only acts as a power source for wheel temperature monitoring, but also a wheel speed sensor with high sensitivity.
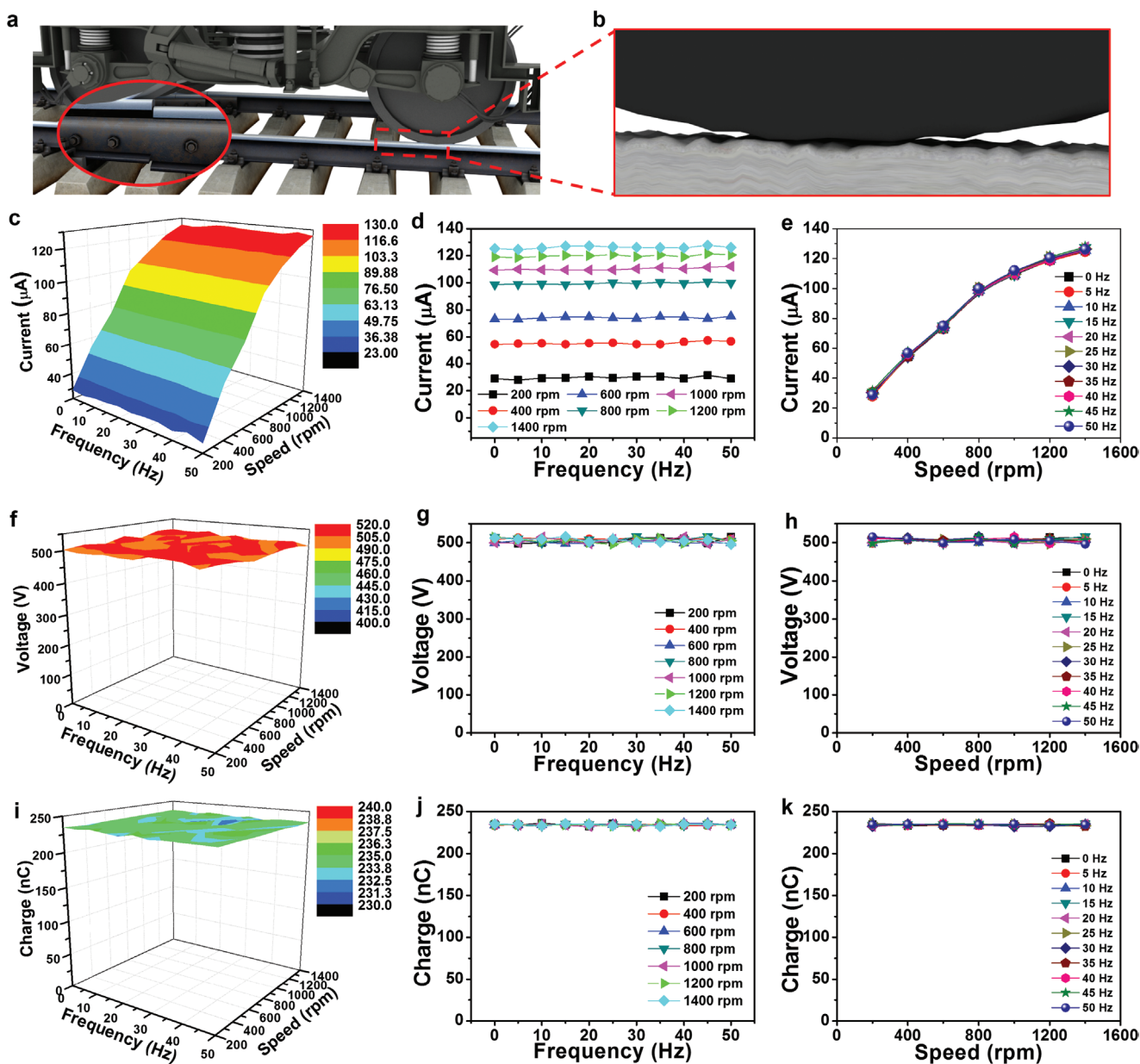
Figure 4. The performance of FF-TENG in vibration environment. The vibration is mainly from a) loose track connection and b) rough surface. c) 3D surface graph and d,e) derived 2D graphs of output current versus both the vibration frequency and rotation speed. Corresponding characterization of f–h) voltage and i–k) transferred charge.

3. Conclusion

In summary, we have presented an FF-TENG for self-powered wheel monitoring. With the structure design, FF-TENG delivers a short-circuit current of 55 µA, open-circuit voltage of 500 V, and charge of 235 nC at rotation speed of 400 rpm. Having remarkable stability in vibration environment, FF-TENG is highly practicable for train wheel energy harvesting. As a result, 140 commercial LEDs can be lighted up and a self-powered wheel monitoring has been developed with FF-TENG as power source. It is worth mentioning that the power management circuit based on LTC 3588 in this system is extremely effective rather than traditional rectifiers. Additionally,

FF-TENG can be utilized as an extraordinarily sensitive wheel speed sensor. This work could be extensively applied on wheel energy harvesting, pushing forward the development of intelligent transportation.

4. Experimental Section

Fabrication of Free-Fixed Triboelectric Nanogenerator: The framework of the device was constructed by acrylic sheets. First, a 6 mm acrylic sheet was cut into a disc with diameter of 150 mm, as the base of rotator. This process was taken by a laser cutting machine (Universal Laser Systems PLS6MW). Then, a piece of copper film was adhered to the acrylic disc, and carved into blade shape, as two electrodes. In details, each blade's
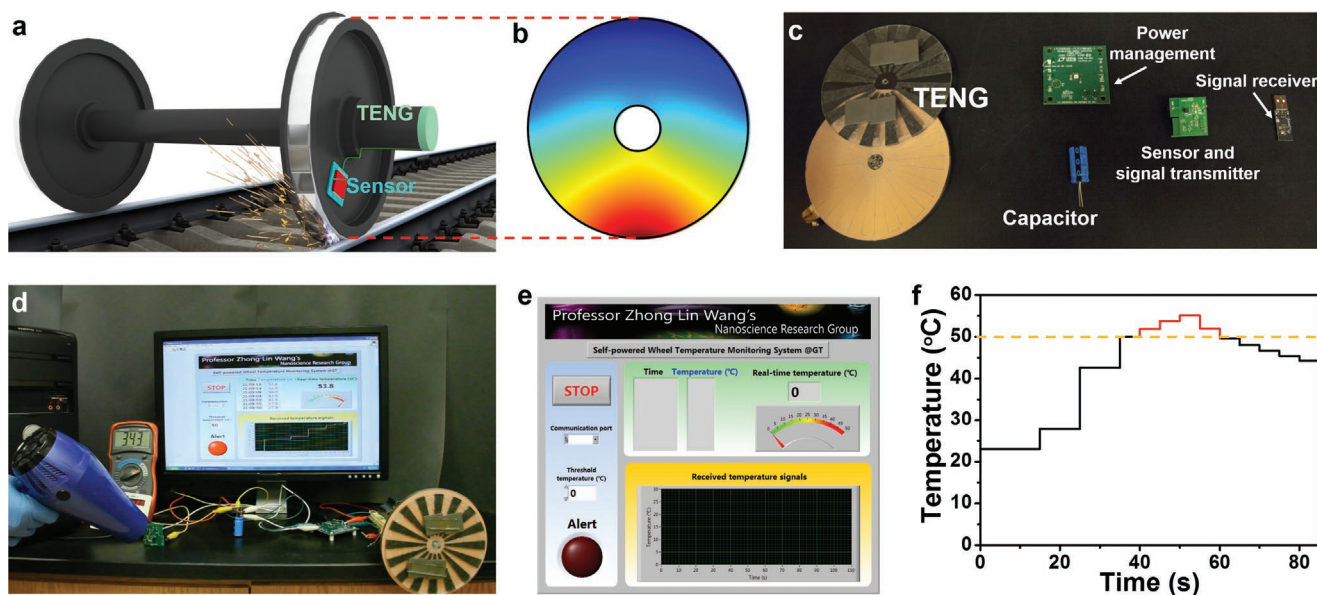
Figure 5. a) Schematic illustration of wheel braking and b) the simulated distribution of temperature. c) Photograph of the self-powered wheel temperature monitoring system components. d) Application of FF-TENG powering a wireless temperature sensor. e) The interface of self-powered wheel temperature monitoring system. f) The temperature change process with alarm threshold value of 50 °C.

outer diameter was 67.5 mm and inner diameter was 12.5 mm, with an angle of 11.25°. In another words, the disc was separated into 32 parts. Next, PTFE of 50 μm was adhered on the electrodes. Finally, an acrylic tube with outer diameter of 150 mm was fixed with the disc by glue to protect the inner. Thus, the rotator was finished. The stator was made by an acrylic disc (135 mm in diameter), and cut by the laser cutting machine. Then, PU foam was cut by knife into blade shape; the same size with each blade of electrodes. And, the PU blades were alternately adhered on the stator disc. Finally, two sets of magnets were fixed on the other side of stator disc. Each set of magnets included two magnets with inverse polarity upward. Thus, the stator was finished. Combining the stator and the rotator together, a free-fixed triboelectric nanogenerator was fabricated.

Characterization: Keithley 6514 system electrometer was used to measure the short-circuit current, the open-circuit voltage, and the transferred charge. A software platform was programmed using LabVIEW to achieve real-time data acquisition and analysis. The vibration was provided by the vibration provider (ET-126B-4) with signal from signal generator (PA-119).

Supporting Information

Supporting Information is available from the Wiley Online Library or from the author.

Conflict of Interest

The authors declare no conflict of interest.

[1] T. C. Barker, M. Robbins, *A History of London Transport: The Nineteenth Century*, Routledge, Abingdon, UK **2006**.

[2] L. Jin, B. B. Zhang, L. Zhang, W. Q. Yang, *Nano Energy* **2019**, *66*, 104086.

[3] P. Neirotti, A. De Marco, A. C. Cagliano, G. Mangano, F. Scorrano, *Cities* **2014**, *38*, 25.

[4] Y. Hu, C. Xu, Y. Zhang, L. Lin, R. L. Snyder, Z. L. Wang, *Adv. Mater.* **2011**, *23*, 4068.

[5] W. Wu, X. Cao, J. Zou, Y. Ma, X. Wu, C. Sun, M. Li, N. Wang, Z. Wang, L. Zhang, *Adv. Funct. Mater.* **2018**, *29*, 1806331.

[6] J. Qian, D. S. Kim, D. W. Lee, *Nano Energy* **2018**, *49*, 126.

[7] S. Xu, W. Liu, B. Hu, X. Wang, *Nano Energy* **2019**, *58*, 803.

[8] H. Zhang, H. Su, L. Zhang, B. Zhang, F. Chun, X. Chu, W. He, W. Yang, *J. Power Sources* **2016**, *331*, 332.

[9] H. Zhang, L. Zhang, J. Chen, H. Su, F. Liu, W. Yang, *J. Power Sources* **2016**, *315*, 120.

[10] F. Liu, Z. Wang, H. Zhang, L. Jin, X. Chu, B. Gu, H. Huang, W. Yang, *Carbon* **2019**, *149*, 105.

[11] Z. Wang, H. Su, F. Liu, X. Chu, C. Yan, B. Gu, H. Huang, T. Yang, N. Chen, Y. Han, W. Deng, H. Zhang, W. Yang, *Electrochim. Acta* **2019**, *307*, 302.

[12] M. Shirvanimoghaddam, K. Shirvanimoghaddam, M. M. Abolhasani, M. Farhangi, V. Zahiri Barsari, H. Liu, M. Dohler, M. Naebe, *IEEE Access* **2019**, *7*, 94533.

[13] F. Wortmann, K. Flüchter, *Bus. Inf. Syst. Eng.* **2015**, *57*, 221.

[14] J. Gubbi, R. Buyya, S. Marusic, M. Palaniswami, *Future Gener. Comput. Syst.* **2013**, *29*, 1645.

[15] Z. L. Wang, *Nano Energy* **2019**, *58*, 669.

[16] L. Jin, W. Deng, Y. Su, Z. Xu, H. Meng, B. Wang, H. Zhang, B. Zhang, L. Zhang, X. Xiao, M. Zhu, W. Yang, *Nano Energy* **2017**, *38*, 185.

[17] B. Zhang, J. Chen, L. Jin, W. Deng, L. Zhang, H. Zhang, M. Zhu, W. Yang, Z. L. Wang, *ACS Nano* **2016**, *10*, 6241.

[18] L. Jin, J. Chen, B. Zhang, W. Deng, L. Zhang, H. Zhang, X. Huang, M. Zhu, W. Yang, Z. L. Wang, *ACS Nano* **2016**, *10*, 7874.

[19] C. Chen, L. Chen, Z. Wu, H. Guo, W. Yu, Z. Du, Z. L. Wang, *Mater. Today* **2020**, *32*, 84.

[20] X. Chen, L. Gao, J. Chen, S. Lu, H. Zhou, T. Wang, A. Wang, Z. Zhang, S. Guo, X. Mu, Z. L. Wang, Y. Yang, *Nano Energy* **2020**, *69*, 104440.

[21] X. Liang, T. Jiang, G. Liu, Y. Feng, C. Zhang, Z. L. Wang, *Energy Environ. Sci.* **2020**, *13*, 277.

[22] B. Zhang, L. Zhang, W. Deng, L. Jin, F. Chun, H. Pan, B. Gu, H. Zhang, Z. Lv, W. Yang, Z. L. Wang, *ACS Nano* **2017**, *11*, 7440.

[23] J. Chen, G. Zhu, W. Yang, Q. Jing, P. Bai, Y. Yang, T. C. Hou, Z. L. Wang, *Adv. Mater.* **2013**, *25*, 6094.

[24] S. Xu, L. Zhang, W. Ding, H. Guo, X. Wang, Z. L. Wang, *Nano Energy* **2019**, *66*, 104165.

[25] S. Xu, W. Ding, H. Guo, X. Wang, Z. L. Wang, *Adv. Energy Mater.* **2019**, *9*, 1900772.

[26] S. L. Zhang, Q. Jiang, Z. Wu, W. Ding, L. Zhang, H. N. Alshareef, Z. L. Wang, *Adv. Energy Mater.* **2019**, *9*, 1900152.

[27] X. Zhang, M. Yu, Z. Ma, H. Ouyang, Y. Zou, S. L. Zhang, H. Niu, X. Pan, M. Xu, Z. Li, Z. L. Wang, *Adv. Funct. Mater.* **2019**, *29*, 1900327.

[28] T. Guo, G. Liu, Y. Pang, B. Wu, F. Xi, J. Zhao, T. Bu, X. Fu, X. Li, C. Zhang, Z. L. Wang, *Extreme Mech. Lett.* **2018**, *18*, 1.

[29] C. R. Bowen, M. H. Arafa, *Adv. Energy Mater.* **2015**, *5*, 1401787.

[30] Y. Mao, D. Geng, E. Liang, X. Wang, *Nano Energy* **2015**, *15*, 227.

[31] M. A. Parvez Mahmud, N. Huda, S. H. Farjana, M. Asadnia, C. Lang, *Adv. Energy Mater.* **2018**, *8*, 1701210.

[32] S. H. Sung, Y. S. Kim, D. J. Joe, B. H. Mun, B. K. You, D. H. Keum, S. K. Hahn, M. Berggren, D. Kim, K. J. Lee, *Nano Energy* **2018**, *51*, 102.

[33] H. Yu, X. He, W. Ding, Y. Hu, D. Yang, S. Lu, C. Wu, H. Zou, R. Liu, C. Lu, Z. L. Wang, *Adv. Energy Mater.* **2017**, *7*, 1700565.

[34] S. Li, D. Liu, Z. Zhao, L. Zhou, X. Yin, X. Li, Y. Gao, C. Zhang, Q. Zhang, J. Wang, Z. L. Wang, *ACS Nano* **2020**, *14*, 2475.

[35] S. L. Zhang, M. Xu, C. Zhang, Y.-C. Wang, H. Zou, X. He, Z. Wang, Z. L. Wang, *Nano Energy* **2018**, *48*, 421.

[36] J. Chen, J. Yang, Z. Li, X. Fan, Y. Zi, Q. Jing, H. Guo, Z. Wen, K. C. Pradel, S. Niu, Z. L. Wang, *ACS Nano* **2015**, *9*, 3324.

[37] Z. L. Wang, T. Jiang, L. Xu, *Nano Energy* **2017**, *39*, 9.

[38] G. Zhu, J. Chen, T. Zhang, Q. Jing, Z. L. Wang, *Nat. Commun.* **2014**, *5*, 3426.

[39] K. Zhao, X. Wang, Y. Yang, *Adv. Mater. Technol.* **2017**, *2*, 1600233.

[40] Y. Jie, J. Ma, Y. Chen, X. Cao, N. Wang, Z. L. Wang, *Adv. Energy Mater.* **2018**, *8*, 1802084.

[41] I. W. Tcho, S. B. Jeon, S. J. Park, W. G. Kim, I. K. Jin, J. K. Han, D. Kim, Y. K. Choi, *Nano Energy* **2018**, *50*, 489.